

Synthesis and Structure–Activity Relationships of 5,6,7-Substituted Pyrazolopyrimidines: Discovery of a Novel TSPO PET Ligand for Cancer Imaging

Dewei Tang,^{†,‡} Eliot T. McKinley,^{†,§} Matthew R. Hight,^{†,||} Md. Imam Uddin,^{†,▽} Joel M. Harp,^{⊥,‡} Allie Fu,[†] Michael L. Nickels,^{†,▽} Jason R. Buck,^{†,▽} and H. Charles Manning^{*,†,‡,§,▽,○,◆}

[†]Vanderbilt University Institute of Imaging Science (VUIIS), Vanderbilt University Medical Center, Nashville, Tennessee, United States

[‡]Program in Chemical and Physical Biology, Vanderbilt University Medical Center, Nashville, Tennessee, United States

[§]Department of Biomedical Engineering, Vanderbilt University, Nashville, Tennessee, United States

^{||}Interdisciplinary Materials Science Program, Department of Physics & Astronomy, Vanderbilt University, Nashville, Tennessee, United States

[⊥]Department of Biochemistry, Vanderbilt University Medical Center, Nashville, Tennessee, United States

[#]Department of Biological Sciences, Vanderbilt University, Nashville, Tennessee, United States

[▽]Department of Radiology and Radiological Sciences, Vanderbilt University Medical Center, Nashville, Tennessee, United States

[○]Vanderbilt Ingram Cancer Center, Vanderbilt University Medical Center, Nashville, Tennessee, United States

[◆]Department of Neurosurgery, Vanderbilt University Medical Center, Nashville, Tennessee, United States

S Supporting Information

ABSTRACT: Focused library synthesis and structure–activity relationship development of 5,6,7-substituted pyrazolopyrimidines led to the discovery of 2-(5,7-diethyl-2-(4-(2-fluoroethoxy)phenyl)pyrazolo[1,5-*a*]pyrimidin-3-yl)-*N,N*-diethylacetamide (**6b**), a novel translocator protein (TSPO) ligand exhibiting a 36-fold enhancement in affinity compared to another pyrazolopyrimidine-based TSPO ligand, **6a** (DPA-714). Radiolabeling with fluorine-18 (¹⁸F) facilitated production of 2-(5,7-diethyl-2-(4-(2-[¹⁸F]fluoroethoxy)phenyl)pyrazolo[1,5-*a*]pyrimidin-3-yl)-*N,N*-diethylacetamide (¹⁸F-**6b**) in high radiochemical yield and specific activity. In vivo studies of ¹⁸F-**6b** were performed which illuminated this agent as an improved probe for molecular imaging of TSPO-expressing cancers.

■ INTRODUCTION

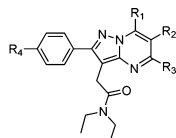
There remains a critical need to develop and rigorously validate molecular imaging biomarkers that aid tumor diagnosis, predict clinical outcome, and quantify response to therapeutic interventions. Imaging techniques routinely used in clinical oncology include magnetic resonance imaging (MRI), X-ray computed tomography (CT), ultrasound imaging (US), and positron emission tomography (PET). Of these, the sensitivity and quantitative nature of PET, coupled with the ability to readily produce biologically active compounds bearing positron-emitting isotopes (e.g., ¹¹C, ¹⁸F), renders PET imaging as one of the most attractive techniques for detecting tumors and profiling their molecular features. By far, the most widely used PET tracer in clinical oncology is 2-deoxy-2-[¹⁸F]fluoro-D-glucose (¹⁸F-FDG), a probe that accumulates in tissue as a function of glucose utilization. PET using ¹⁸F-FDG is a powerful approach for tumor detection in many organ sites. However, not all tumors exhibit elevated glucose avidity, and ¹⁸F-FDG uptake can be affected by a plethora of normal metabolic processes. Furthermore, tumor imaging can be confounded by ¹⁸F-FDG uptake in normal tissues such as healthy brain. These issues highlight an unmet need to explore and validate additional molecular targets for cancer imaging.

Our laboratory has explored translocator protein (TSPO) expression as a target for molecular imaging of cancer.^{1–5} Formerly referred to as peripheral benzodiazepine receptor (PBR), TSPO is an 18 kDa protein typically localized to the outer mitochondria membrane. TSPO participates in the regulation of numerous cellular processes, including steroid biosynthesis, cholesterol metabolism, apoptosis, and cellular proliferation.⁶ In normal tissues, TSPO tends to be expressed in those that produce steroids and those that are mitochondrial-enriched such as myocardium, skeletal muscle, and renal tissue. Tissues such as liver and brain exhibit comparatively modest expression.⁶ While classically exploited as a target in neuroscience, elevated TSPO expression is also observed in many cancers.⁷ In oncology, TSPO expression is typically linked with disease progression and diminished survival and is a hallmark of aggressive and potentially metastatic tumors.⁷ For this reason, our laboratory has explored the use of TSPO imaging ligands within the context of colon cancer,¹ breast cancer,² and glioma,^{4,5} as these agents could potentially serve as useful cancer imaging biomarkers. We recently reported the first

Received: February 5, 2013



Table 1. Affinity, Lipophilicity, and Molecular Weight of Pyrazolopyrimidines



compd	R ₁	R ₂	R ₃	R ₄	MW	log P _{7.5}	K _i (nM) ^d
5a ^a	–Me	–H	–Me	–OMe	366.21	2.40	12.23
5b	–Et	–H	–Et	–OMe	394.51	2.84	0.18
5c ^b	–iPr	–H	–iPr	–OMe	422.56	2.98	>500
5d	–Me	–Me	–Me	–OMe	380.48	2.45	93.75
5e	–Me	–Et	–Me	–OMe	394.51	2.78	157.14
5f	–Me	–CH ₂ C(O)CH ₃	–Me	–OMe	408.49	2.57	200.89
5g	–Me	–Cl	–Me	–OMe	400.9	2.99	55.36
6a ^c	–Me	–H	–Me	–OCH ₂ CH ₂ F	398.47	2.12	9.73
6b	–Et	–H	–Et	–OCH ₂ CH ₂ F	426.53	2.50	0.27 ^e
6c	–iPr	–H	–iPr	–OCH ₂ CH ₂ F	454.58	2.73	>500
6d	–Me	–Me	–Me	–OCH ₂ CH ₂ F	412.5	2.47	83.04
6e	–Me	–Et	–Me	–OCH ₂ CH ₂ F	426.53	2.53	276.79
6f	–Me	–CH ₂ C(O)CH ₃	–Me	–OCH ₂ CH ₂ F	440.51	2.07	251.79
6g	–Me	–Cl	–Me	–OCH ₂ CH ₂ F	432.92	2.55	67.86

^aDPA-713, see ref 8–11. ^bSee ref 12. ^cDPA-714, see refs 8–10,13. ^dCompetitive binding against ³H-PK 11195 in C6 glioma cell lysate. ^eK_i versus ³H-flunitrazepam >10000 nM.

utilizations of the PET agents *N*-[¹⁸F]fluoroacetyl-*N*-(2,5-dimethoxybenzyl)-2-phenoxyaniline (¹⁸F-PBR06)⁵ and *N,N*-diethyl-2-(2-(4-(2-[¹⁸F]fluoroethoxy)phenyl)-5,7-dimethylpyrazolo[1,5-*a*]pyrimidin-3-yl)acetamide (¹⁸F-DPA-714)⁴ for quantitative assessment of TSPO expression in preclinical glioma. In these proof-of-principle PET imaging studies, tumors were detectable among surrounding normal brain and, importantly, TSPO levels could be quantitatively assayed in tumors using compartmental analysis of the PET data.^{4,5} However, drawbacks were observed with both agents in this context, including tracer accumulation in normal brain that reached levels potentially sufficient to prevent detection of gliomas with modest TSPO expression. Both tracers also exhibited significant metabolism *in vivo*, which required correction of plasma input functions for quantitative analysis. While illustrating the potential of TSPO PET to detect tumors in brain, these studies prompted our desire to develop novel TSPO PET ligands with improved properties for cancer imaging.

The goal of this study was to determine whether optimization of the pyrazolopyrimidine scaffold, specifically at the 5-, 6-, and 7-positions, would yield TSPO ligands with greater affinity and potentially serve as more robust PET imaging ligands *in vivo*. These experiments led to the discovery of 2-(5,7-diethyl-2-(4-(2-[¹⁸F]fluoroethoxy)phenyl)pyrazolo[1,5-*a*]pyrimidin-3-yl)-*N,N*-diethylacetamide (**6b**), a novel TSPO-selective ligand that exhibits a surprising 36-fold enhancement in affinity compared to another pyrazolopyrimidine, **6a** (DPA-714). An appropriate analogue of **6b**, compound **7**, could be radiolabeled with fluorine-18 (¹⁸F) to yield the novel TSPO PET ligand 2-(5,7-diethyl-2-(4-(2-[¹⁸F]fluoroethoxy)phenyl)pyrazolo[1,5-*a*]pyrimidin-3-yl)-*N,N*-diethylacetamide (¹⁸F-**6b**), which was subsequently evaluated *in vivo* in healthy rats and a preclinical model of glioma. ¹⁸F-**6b** exhibited negligible accumulation in normal brain, yet robust accumulation in tumor tissue, which facilitated excellent imaging contrast. Overall, these studies illuminate ¹⁸F-**6b** as a promising, novel

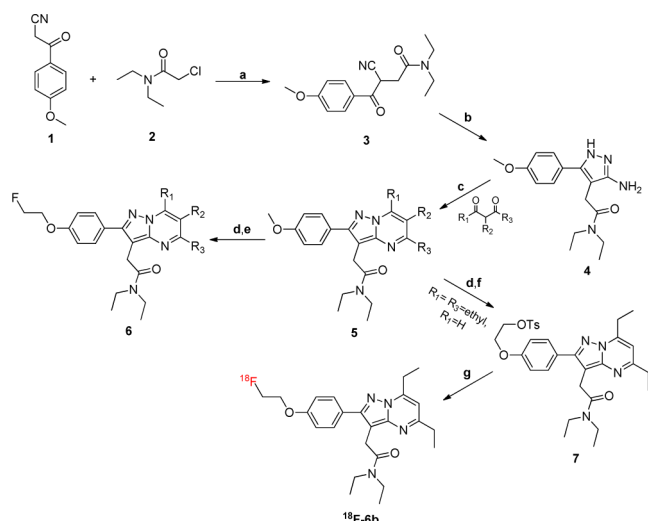
PET ligand for evaluating TSPO expression in tumors and potentially other diseases.

RESULTS AND DISCUSSION

Chemistry. MAOS of 5,6,7-Substituted Pyrazolopyrimidine Library. A library of structurally diverse pyrazolopyrimidines (Table 1) was assembled using a microwave-assisted organic synthesis (MAOS) method that prioritized points of divergence at the 5-R₃, 6-R₂, and 7-R₁ positions on the core pyrazolopyrimidine scaffold. Members of this library were formed through condensation of a pyrazole core (**4**) with various substituted diones.¹² Entries in Table 1 fall into two distinct series (**5** and **6**), with seven compounds (**a–g**) per series. Each compound within the series results from one of seven diones utilized, while each series is differentiated by the installation of a unique surrogate imaging handle at the 4-position (R₄) of the 2-phenyl group pendant to the core scaffold. Series 5 entries (**5a–5g**) feature a methoxy group at R₄ and include a previously reported pyrazolopyrimidine, **5a** (DPA-713),^{8–11} while series 6 entries (**6a–6g**) feature a 2-fluoroethoxy group at R₄ and include **6a**.^{8–10,13} Given our ultimate goal of developing novel PET imaging ligands, coupled with an interest in expanding structure–activity relationships (SAR) around the 5,6,7-substituted pyrazolopyrimidine core, we rationalized that maintaining the surrogate imaging handles of future representative imaging probes would accelerate the development of novel agents.

The overall synthetic methodology is presented in Scheme 1.¹² Here, compound **4**, bearing a 3-amino-1*H*-pyrazole core, was accessible in two steps using MAOS from commercially available phenylpropanenitrile **1** and chloroacetamide **2**. From **4**, the synthesis diverges at the condensation step with a series of unique diones to yield the “five” series of pyrazolopyrimidines (**5a–5g**) that mimic analogous ¹¹C-based PET probes with an R₄-OMe. Subsequently, compounds **6a–6g** were achieved by cleavage of methoxy group followed by microwave-assisted ether synthesis with 2-fluoroethyl-4-methylbenzenesulfonate which yielded an R₄-2-fluoroethoxy surrogate

Scheme 1. Synthetic Methodology Utilized to Generate a Focused Library of 5,6,7-Substituted Pyrazolopyrimidines and ^{18}F -6b**^a**



^aReagents and conditions: (a) NaOH, NaI, microwave, 80 °C, 40 min, 80% EtOH in H₂O, 70%; (b) hydrazine, AcOH, microwave, 90 °C, 40 min, EtOH, 42%; (c) microwave, 140–190 °C, 45 min, EtOH, 10–90%; (d) HTPB, microwave, 110 °C, 40 min, aqueous HBr; (e) NaH, 2-fluoroethyl-4-methylbenzenesulfonate, microwave, 120 °C, 30 min, dry THF; (f) ethylene di(*p*-toluenesulfonate), NaH, microwave, 120 °C, 30 min, dry THF, 45%; (g) fluoride-18 ion, K⁺-K_{2.2.2}/K₂CO₃, 99 °C, 20 min, dry DMSO.

imaging handle to mimic ^{18}F -labeled PET probes (Table 1). The library developed primarily explored the effects of R₁, R₂, and R₃ substituents that varied in steric bulk. Generally, substituents at R₁ and R₃ mirrored one another and consisted of linear and branched alkyl substituents such as methyl, ethyl, and isopropyl moieties. These substituents were cross-matched with similar groups at the R₂ position, which included hydrogen, methyl, ethyl, chloro, and 2-propanone.

Lipophilicity. Lipophilicity of series 5 and 6 were evaluated at pH = 7.5 (log *P*_{7.5}) using reversed phase HPLC¹⁴ and is tabulated in Table 1. The values for library entries varied from 2.0 to 3.0 for both series and correlated predictably with dione structure, where polarity and hydrocarbon content of the R₁–R₃ substituents appeared to be key determinants. In both series, analogues a, d, and f, with R₁–R₃ combinations of hydrogen, methyl, and 2-propanone, proved the least lipophilic. Introduction of ethyl groups at R₁, R₂, or R₃ increased log *P*_{7.5} values accordingly, as with analogues b and e, which ranged from 2.50 to 2.84. The most lipophilic analogues proved to be c and g (log *P*_{7.5} = 2.55–2.99), with isopropyl groups at the R₁ and R₃ positions or chlorine at R₂.

Interestingly, of the two series, series 5 (R₄ = OMe) tended to be more lipophilic than series 6 (R₄ = OCH₂CH₂F). Overall, the library entries exhibited lipophilicities (2.07–2.99) suitable for in vivo imaging,¹⁵ where potential agents must be sufficiently membrane penetrant to bind intracellular targets such as TSPO.

Biological Testing. Binding Affinity in Cancer Cell Lysate and SAR Analysis. To evaluate binding of the library entries to TSPO, radioligand displacement was carried out in rat glioma cell lysate (C6) using *N*-(*sec*-butyl)-1-(2-chlorophenyl)-*N*-methyl-³H-isoquinoline-3-carboxamide (³H-PK 11195).^{4,5} Affinities of library members are expressed as *K*_i (nM) values in

Table 1. Encompassing modifications at R₁–R₄, both series exhibited a spectrum of *K*_i values that spanned micromolar to subnanomolar affinity. As expected, replacing the 4-methoxy with 4-(2-fluoroethoxy) at the R₄ position had minimal impact upon TSPO affinity, as similar SAR trends emerged within series 5 and 6. In contrast, R₁, R₂, and R₃ modification led to major impacts upon affinity. Although the R₁ and R₃ positions showed intolerance to steric bulk beyond ethyl, a surprising level of improvement in affinity could be realized by replacing methyl with ethyl at the R₁ and R₃ positions. For example, subnanomolar affinities (*K*_i) were observed for analogues **5b** (0.18 nM) and **6b** (0.27 nM), which represent major improvements over their respective leads, **5a** (12.23 nM) and **6a** (9.73 nM) (Table 1), as well as another high-affinity TSPO ligand, *N*-(2-methoxybenzyl)-*N*-(4-phenoxy-pyridin-3-yl)-acetamide (PBR28) (4.0 nM).¹⁶ Increasing the R₁ and R₃ to a bulkier isopropyl group proved detrimental, with *K*_i values for both **5c** and **6c** greater than 500 nM. Overall, the R₂ position was less tolerant to steric or electron density deviations from hydrogen in these studies. Substitution of the nascent R₂ hydrogen (**5a**, **6a**) with methyl (**5d**, 93.75 nM; **6d**, 83.04 nM) decreased affinity approximately 10-fold with respect to their parent compounds, **5a** and **6b**, respectively; this trend was more dramatic with ethyl substitution (**5e**, 157.14 nM; **6e**, 276.79 nM). Introduction of polarity at the R₂ position with 2-propanone (**5f**, 200.89 nM; **6f**, 251.79 nM) bore similar adverse effects upon affinity. Somewhat less dramatic decreases in affinity were observed upon halogen substitution at R₂ with chlorine (**5g**, 55.36 nM; **6g**, 67.86 nM). Given the size of chlorine atom, lying between methyl and ethyl, it is reasonable that the *K*_i of entries **5g** and **6g** are only slightly worse than those with alkyl substituents at the R₂ position (Table 1). Overall, these experiments illuminated 5,7-diethyl, 6-hydrogen substitution as the optimal pattern in this series to impart improved affinity. Additionally, the studies also suggested that an analogue could be produced for PET imaging using either fluorine-18 (**6b**) or carbon-11 (**5a**) substitution on the R₄ position with minimal effect on TSPO affinity and only minor effect on lipophilicity. Because fluorine-18 has a significantly longer half-life than carbon-11 (109.8 min vs 20.4 min), we elected to carry compound **6b** forward for further characterization. The selectivity of compound **6b** for TSPO over the central benzodiazepine receptor (CBR) was evaluated using radioligand displacement of the CBR ligand ³H-flunitrazepam in rat cerebral cortex membranes (Table 1). Unlike the displacement studies with ³H-PK 11195, compound **6b** demonstrated poor affinity for CBR (*K*_i > 10000 nM), indicating TSPO selectivity.

Radiochemistry. Radioligand Precursor Preparation and Radiosynthesis. To produce ^{18}F -**6b**, we synthesized precursor (**7**), a tosylated intermediate prepared from **5b** in two steps with an overall yield of approximately 45% (Scheme 1). Nucleophilic fluorination of **7** with fluorine-18 was then performed (Scheme 1) in anhydrous dimethyl sulfoxide at 165 °C for 5 min. Purification of ^{18}F -**6b** was carried out with preparative HPLC using 10 mM sodium phosphate buffer (pH 6.7) in ethanol (47.5/52.5, v/v). The retention time of ^{18}F -**6b** was 12 min according to gamma detection and corresponded to the UV retention time of nonradioactive **6b**. Radiochemical purity was consistently greater than 99%, with specific activity consistently greater than 4203 Ci/mmol (156 TBq/mmol) (*n* = 33).

Imaging Studies. Uptake of ^{18}F -6b** in C6 Glioma.** The in vivo performance of ^{18}F -**6b** was evaluated in glioma-bearing Wistar rats using microPET imaging, with a typical study shown in Figure 1. MRI (T_2 -weighted) was used to localize tumors

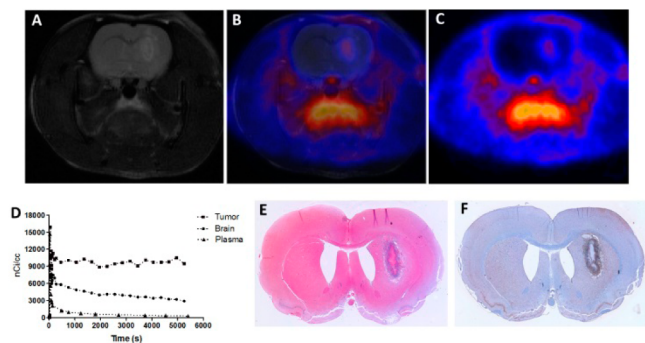


Figure 1. PET imaging of preclinical glioma using ^{18}F -**6b**.

and for registration of anatomical features with PET^{4,5} (Figure 1A). Dynamic PET imaging with ^{18}F -**6b** illustrated that the majority of tracer uptake in the brain was localized to the tumor, with very modest accumulation in the adjacent, normal brain (Figure 1B,C). The tumor-selective uptake characteristics of ^{18}F -**6b** afforded excellent imaging contrast between tumor and normal tissue. In addition to the tumor, accumulation of ^{18}F -**6b** was observed outside of the brain in olfactory epithelium and the Harderian glands, as well as the tongue, where TSPO expression is elevated.⁷ Figure 1D illustrates time-activity curves (TACs) that were typical of eight representative studies for tumor, normal brain, and plasma over a 90 min dynamic acquisition. We found that ^{18}F -**6b** was rapidly delivered to tumor and normal brain but cleared tumor tissues at a much slower rate than normal brain. After an initial spike in radioactivity consistent with tracer injection and rapid distribution, ^{18}F -**6b** quickly cleared from the plasma. To validate the PET, imaging-matched brains were processed for post-mortem staining and immunohistochemistry. We observed close agreement between tumor tissue (H&E, Figure 1E), elevated TSPO expression by immunohistochemistry (Figure 1F), and tumor accumulation of ^{18}F -**6b** accumulation (Figure 1C). To more quantitatively compare the performance of ^{18}F -**6b** to ^{18}F -**6a**, we conducted dynamic PET using ^{18}F -**6b** in a cohort of tumor-bearing rats ($n = 5$) and carried out pharmacokinetic modeling of the PET data, similar to our previous studies.^{4,5} We found that ^{18}F -**6b** demonstrated a higher ratio of total distribution volume (V_T) between tumor and normal brain (6.0, $n = 5$) when compared to ^{18}F -**6a** (3.9, $n = 11$),⁴ which resulted in greater signal-to-noise between tumor and surround normal brain.

Characterization of ^{18}F -6b** Radiometabolites in Plasma.** Analogous to our previous work,⁴ radio-HPLC was used to evaluate metabolism of ^{18}F -**6b** in plasma at multiple time points during the PET scanning period (2, 12, 30, 60, 90 min) (Supporting Information (SI) Figure 1). Parent compound (^{18}F -**6b**) was the only radioactive species detected in plasma at all time points, suggesting a lack of circulating ^{18}F -**6b** metabolites observed over a 90 min period. This behavior contrasted the in vivo performance of ^{18}F -**6a**, where we previously observed up to 30% metabolism within the first 12 min post-administration.⁴ Potentially, the apparent improved stability of ^{18}F -**6b** over ^{18}F -**6a** may stem from the rapid

clearance of ^{18}F -**6b** from plasma, rendering detection of low levels of metabolites challenging with HPLC.

Biodistribution and Specific Binding of ^{18}F -6b** in Rats.** The biodistribution and TSPO-specificity of ^{18}F -**6b** was evaluated in normal tissues. Tissue samples were harvested 60 min after infusion of ^{18}F -**6b**. The radioactivity of harvested tissue was measured using standard analytical methods and recorded as percentage of the injected dose per gram of tissue (%ID/g) (SI Figure 2A). Consistent with known TSPO densities,⁷ we observed elevated accumulation of ^{18}F -**6b** in spleen, heart, kidney, and lung.¹⁷ Moderate uptake was also observed in liver, colon, small bowel, and stomach. Very minor accumulation was observed in the brain, testes, skull, and skeletal muscle. At 60 min postadministration of tracer, very little radioactivity was observed in biological fluids such as whole blood or urine.

To evaluate the specific binding of ^{18}F -**6b** in normal tissue, we carried out a similar 60 min biodistribution assay that included a bolus infusion of nonradioactive **6b** (10 mg/kg) at 30 min (SI Figure 2B). With displacement, we observed that activity in the organs exhibiting the greatest accumulation of ^{18}F -**6b**, such as spleen, heart, kidney, and lung, was reduced to background levels, indicating near complete displacement and reversible binding in healthy tissue. Organs that exhibited low to moderate accumulation of ^{18}F -**6b** without displacement, such as muscle or liver, were essentially unchanged with displacement, suggesting that the low to moderate tracer accumulation in these tissues may reflect nonspecificity. Interestingly, activity found in the urine did not follow this trend and was elevated with displacement, suggesting that blocking TSPO with nonradioactive **6b** altered the excretion profile of the agent. Overall, the results indicate a high degree of specific binding and reversibility of ^{18}F -**6b** to TSPO in healthy tissues.

Crystallography. **6b** was recrystallized from hot acetonitrile and ethanol (95%) by slow evaporation at room temperature and characterized by diffractometry. **6b** demonstrated two ethyl branches at the 5- and 7-positions of the pyrazolopyrimidine ring, corresponding to the structure elucidated from NMR spectroscopy. The crystal structure also revealed three distinct planar entities, the pyrazolopyrimidine ring, the phenyl ring, and the amide group (SI Figure 3).

CONCLUSION

In this study, we found that the 5,6,7-substitution pattern is a critical determinant of TSPO affinity among pyrazolopyrimidines. Experiments shown here led to the discovery of **6b**, a TSPO ligand exhibiting significantly increased affinity compared to **6a** and TSPO ligands derived from other chemical entities.¹⁸ Furthermore, in addition to improved TSPO affinity, compound **6b** was TSPO-selective, exhibiting negligible binding affinity to CBR. Analogue 7 of **6b** could be radiolabeled with fluorine-18 to yield ^{18}F -**6b**. Suggesting its potential as a probe for cancer imaging, preclinical imaging studies demonstrated robust accumulation of ^{18}F -**6b** in tumor tissue and negligible accumulation in normal brain. Overall, these studies illuminate ^{18}F -**6b** as a promising, novel PET ligand for evaluating TSPO expression in tumors and potentially other diseases.

■ ASSOCIATED CONTENT

● Supporting Information

Synthetic and analytical results for all compounds; methods; supplemental figures. This material is available free of charge via the Internet at <http://pubs.acs.org>.

■ AUTHOR INFORMATION

Corresponding Author

*Phone: 615-322-3793; Fax: 615-322-0734; E-mail: henry.c.manning@vanderbilt.edu. Address: Vanderbilt University Institute of Imaging Science (VUIS), 1161 21st Avenue South, AA1105 MCN, Nashville, TN 37232-2310.

Author Contributions

Dr. Manning directed and designed the study. Mr. Tang performed the synthetic chemistry and, along with Mr. McKinley, Mr. Hight, and Dr. Buck, performed the imaging experiments. Dr. Nickels performed the radiochemistry, Dr. Uddin and Dr. Harp carried out the crystallography. All authors participated in writing or editing the manuscript.

Notes

The authors declare no competing financial interest.

■ ACKNOWLEDGMENTS

We acknowledge funding from the National Institutes of Health (K25 CA127349, P50 CA128323, S10 RR17858, U24 CA126588, 1R01 CA163806), The Kleberg Foundation, and The Lustgarten Foundation. M. Noor Tantawy, George H. Wilson, Dan Colvin, and Yiu-Yin Cheung are acknowledged.

■ REFERENCES

- (1) Deane, N. G.; Manning, H. C.; Foutch, A. C.; Washington, M. K.; Aronow, B. J.; Bornhop, D. J.; Coffey, R. J. Targeted imaging of colonic tumors in *smad3*^{−/−} mice discriminates cancer and inflammation. *Mol. Cancer Res.* **2007**, *5*, 341–349.
- (2) Wyatt, S. K.; Manning, H. C.; Bai, M.; Bailey, S. N.; Gallant, P.; Ma, G.; McIntosh, L.; Bornhop, D. J. Molecular imaging of the translocator protein (TSPO) in a pre-clinical model of breast cancer. *Mol. Imaging Biol.* **2010**, *12*, 349–358.
- (3) Manning, H. C.; Goebel, T.; Thompson, R. C.; Price, R. R.; Lee, H.; Bornhop, D. J. Targeted molecular imaging agents for cellular-scale bimodal imaging. *Bioconjugate Chem.* **2004**, *15*, 1488–1495.
- (4) Tang, D.; Hight, M. R.; McKinley, E. T.; Fu, A.; Buck, J. R.; Smith, R. A.; Tantawy, M. N.; Peterson, T. E.; Colvin, D. C.; Ansari, M. S.; Nickels, M.; Manning, H. C. Quantitative preclinical imaging of TSPO expression in glioma using *N,N*-diethyl-2-(2-(4-(2-¹⁸F-fluoroethoxy)phenyl)-5,7-dimethylpyrazolo[1,5-*a*]pyrimidin-3-yl)-acetamide. *J. Nucl. Med.* **2012**, *53*, 287–294.
- (5) Buck, J. R.; McKinley, E. T.; Hight, M. R.; Fu, A.; Tang, D.; Smith, R. A.; Tantawy, M. N.; Peterson, T. E.; Colvin, D.; Ansari, M. S.; Baldwin, R. M.; Zhao, P.; Guleryuz, S.; Manning, H. C. Quantitative, preclinical PET of translocator protein expression in glioma using ¹⁸F-*N*-fluoroacetyl-*N*-(2,5-dimethoxybenzyl)-2-phenoxylaniline. *J. Nucl. Med.* **2011**, *52*, 107–114.
- (6) Papadopoulos, V.; Baraldi, M.; Guilarte, T. R.; Knudsen, T. B.; Lacapere, J. J.; Lindemann, P.; Norenberg, M. D.; Nutt, D.; Weizman, A.; Zhang, M. R.; Gavish, M. Translocator protein (18 kDa): new nomenclature for the peripheral-type benzodiazepine receptor based on its structure and molecular function. *Trends Pharmacol. Sci.* **2006**, *27*, 402–409.
- (7) Batarseh, A.; Papadopoulos, V. Regulation of translocator protein 18 kDa (TSPO) expression in health and disease states. *Mol. Cell. Endocrinol.* **2010**, *327*, 1–12.
- (8) Chauveau, F.; Van Camp, N.; Dolle, F.; Kuhnast, B.; Hinnen, F.; Damont, A.; Boutin, H.; James, M.; Kassiou, M.; Tavitian, B. Comparative evaluation of the translocator protein radioligands ¹¹C-DPA-713, ¹⁸F-DPA-714, and ¹¹C-PK11195 in a rat model of acute neuroinflammation. *J. Nucl. Med.* **2009**, *50*, 468–476.
- (9) Doorduyn, J.; Klein, H. C.; Dierckx, R. A.; James, M.; Kassiou, M.; de Vries, E. F. [¹¹C]-DPA-713 and [¹⁸F]-DPA-714 as new PET tracers for TSPO: a comparison with [¹¹C]-(R)-PK11195 in a rat model of herpes encephalitis. *Mol. Imaging Biol.* **2009**, *11*, 386–398.
- (10) James, M. L.; Fulton, R. R.; Henderson, D. J.; Eberl, S.; Meikle, S. R.; Thomson, S.; Allan, R. D.; Dolle, F.; Fulham, M. J.; Kassiou, M. Synthesis and in vivo evaluation of a novel peripheral benzodiazepine receptor PET radioligand. *Bioorg. Med. Chem.* **2005**, *13*, 6188–6194.
- (11) Sella, S.; Bruni, F.; Costagli, C.; Costanzo, A.; Guerrini, G.; Ciciani, G.; Costa, B.; Martini, C. 2-Arylpyrazolo[1,5-*a*]pyrimidin-3-yl acetamides. New potent and selective peripheral benzodiazepine receptor ligands. *Bioorg. Med. Chem.* **2001**, *9*, 2661–2671.
- (12) Tang, D.; Buck, J. R.; Hight, M. R.; Manning, H. C. Microwave-Assisted Organic Synthesis of a High-Affinity Pyrazolo-pyrimidinyl TSPO Ligand. *Tetrahedron Lett.* **2010**, *51*, 4595–4598.
- (13) Martin, A.; Boisgard, R.; Theze, B.; Van Camp, N.; Kuhnast, B.; Damont, A.; Kassiou, M.; Dolle, F.; Tavitian, B. Evaluation of the PBR/TSPO radioligand [(18F)DPA-714 in a rat model of focal cerebral ischemia. *J. Cereb. Blood Flow Metab.* **2010**, *30*, 230–241.
- (14) Waterhouse, R. N.; Mardon, K.; Giles, K. M.; Collier, T. L.; O'Brien, J. C. Halogenated 4-(phenoxymethyl)piperidines as potential radiolabeled probes for sigma-1 receptors: in vivo evaluation of [¹²⁵I]-1-(iodopropen-2-yl)-4-[(4-cyanophenoxy)methyl]piperidine. *J. Med. Chem.* **1997**, *40*, 1657–1667.
- (15) Pike, V. W. PET radiotracers: crossing the blood–brain barrier and surviving metabolism. *Trends Pharmacol. Sci.* **2009**, *30*, 431–440.
- (16) Owen, D. R.; Howell, O. W.; Tang, S. P.; Wells, L. A.; Bennacef, I.; Bergstrom, M.; Gunn, R. N.; Rabiner, E. A.; Wilkins, M. R.; Reynolds, R.; Matthews, P. M.; Parker, C. A. Two binding sites for [³H]PBR28 in human brain: implications for TSPO PET imaging of neuroinflammation. *J. Cereb. Blood Flow Metab.* **2010**, *30*, 1608–1618.
- (17) Fujimura, Y.; Kimura, Y.; Simeon, F. G.; Dickstein, L. P.; Pike, V. W.; Innis, R. B.; Fujita, M. Biodistribution and radiation dosimetry in humans of a new PET ligand, (18F)-PBR06, to image translocator protein (18 kDa). *J. Nucl. Med.* **2010**, *51*, 145–149.
- (18) Taliani, S.; Pugliesi, I.; Da Settimo, F. Structural Requirements to Obtain Highly Potent and Selective 18 kDa Translocator Protein (TSPO) Ligands. *Curr. Top. Med. Chem.* **2011**, *11* (7), 860–886.